Electronic Supplementary information

Polymorphism and Phase Transformation Tuned Luminescence and Mechanistic Insights in Nonconventional Luminophores

Anze Li, Zihao Zhao, Guangxin Yang, Qiang Zhang, Xiang Chen and Wang Zhang Yuan*

School of Chemistry and Chemical Engineering, Frontiers Science Center for Transformative Molecules, Shanghai Key Lab of Electrical Insulation and Thermal Aging, Shanghai Jiao Tong University, No. 800 Dongchuan Rd., Minhang District, Shanghai 200240, China.
E-mail: wzhyuan@sjtu.edu.cn

Experimental Section

Materials. Trimethylamine (30% in ethanol) was purchased from Shanghai Adamas Reagent Co., Ltd. 1,8-Dibromooctane (98%) was purchased from Shanghai Macklin Biochemical Co., Ltd. 1,10-Dibromodecane was purchased from Meryer (Shanghai) Chemical Technology Co., Ltd. 1,10-Diiododecane was purchased from Shanghai Aladdin Biochemical Technology Co., Ltd. Methanol, ethanol, acetone, diethyl ether and acetonitrile were purchased from Shanghai Adamas Reagent Co., Ltd. Pure water was purchased from Hangzhou Wahaha Group Co., Ltd (Zhejiang, China). All reagents and materials for spectroscopic measurement were purified by recrystallization and/or column chromatography before use to guarantee their purity.

Instrumentation. ^{1}H and ^{13}C NMR spectra were conducted on a Bruker AVANCE III HD 500 Nuclear Magnetic Resonance spectrometer. High-performance liquid chromatography (HPLC) spectra were measured on an ALLIANCE e2695 with Evaporative Light-scattering Detector. X-ray diffraction (XRD) spectra were obtained on a PANalytical Aeris diffractometer. Single-crystal data were acquired from a Bruker D8 VENTURE CMOS Photon II X-ray diffractometer with helios mx multilayer monochrmator Cu Ka radiation (λ = 1.54178 Å). Data collection, unit cell refinement, and data reduction were performed using APEX3 v2019.11-0. The structure was solved by Intrinsic Phasing method and refined by full-matrix least-squares on F2 with anisotropic displacement parameters for the non-H atoms using SHELXTL program package. The hydrogen atoms on carbon were calculated in ideal positions with isotropic displacement parameters set to 1.2×Ueq of the attached atom (1.5×Ueq for methyl hydrogen atoms). The hydrogen atoms bound to nitrogen were located in a ΔF map and refined with isotropic displacement parameters. Prompt and delayed emission spectra, excitation spectra, lifetimes, and quantum efficiencies were measured on an Edinburgh FLS1000 photoluminescence spectrometer. Cryogenic quantum yields were obtained from an Quantaurus-QY Plus. All photographs and videos were taken by a digital camera (Sony α7sII, Japan).

Femtosecond transient absorption (fs-TA) experiments. The fs-TA measurements were conducted with an apparatus and methods detailed previously.[1] A femtosecond regenerative amplified Ti: sapphire laser system was employed for the fs-TA measurements, where the amplifier was seeded with 120 fs laser pulses from an oscillator. The laser probe pulse was generated by directing approximately 5% of the amplified 800 nm pulses through a CaF_2 crystal to produce a white-light continuum (350-800 nm). This probe beam was then split into two components before passing through the sample: one probe beam passed through the sample, while the other was directed to a reference spectrometer to monitor fluctuations in probe beam intensity. The 266 nm laser with 0.5 mW power was selected as the excitation wavelength for measuring 10-Br aqueous solution, while a 266 nm laser with 0.15 mW power was used as excitation wavelength for measuring the 10-Br-a and 10-Br-b polymorphic powders.

Nanosecond transient absorption (ns-TA) Spectroscopy. The ns-TA spectra were recorded using an LP980 laser flash photolysis spectrometer (Edinburgh Instruments, UK). Signal digitization was performed with a Tektronix MDO 3022 oscilloscope. Prior to measurement, all samples were degassed with N_2 for approximately 15 min. Kinetic decay traces and fitting data were processed using L900 software.

Computational study. The computational models were extracted from the corresponding single-crystal data. Time-dependent density functional theory (TD-DFT) with the M06-2X hybrid functional combined with def2-TZVP basis set was applied to calculate the HOMO and LUMO electron densities and energy levels. All TD-DFT calculations were carried out using Gaussian 16. Noncovalent interaction (NCI) analysis, root mean square deviation (RMSD), natural transition orbitals (NTO) with corresponding hole-electron ananlysis were conducted using the Multiwfn package and VMD, based on the wave functions generated by Gaussian 16.[2-4] The spin–orbit coupling (SOC) constants between singlets and triplets were calculated by the Orca 5.0 program.

Synthesis of 1,10-Decanebis(trimethylammonium) dibromide (10-Br). Trimethylamine (30% in ethanol, 2.955 g) and 1,10-dibromodecane (1.800 g, 6.0 mmol) were added in a 100 mL round-bottom flask containing 30 mL of methanol. The mixture underwent vigorous stirring at 35 °C for 48 h. Subsequently, a large amount of diethyl ether was added to precipitate the crude product, which was then collected by filtration. The resulting white precipitate was washed three times with 20 mL of acetone followed by 20 mL of diethyl ether, and then dried under vacuum at 40 °C for 12 h. The dried solids were dissolved in methanol and recrystallized using vapor diffusion in a methanol-diethyl ether system. Then the recrystallized products were further purified using a C18 column, followed by a freeze-drying process to obtain the final solid in a yield of 61.2%. ^{1}H NMR (500 MHz, D_2O, ppm) δ = 3.38 – 3.27 (m, 4H), 3.12 (s, 18H), 1.91 – 1.74 (m, 4H), 1.36 (d, *J* = 21.6 Hz, 12H). ^{13}C NMR (126 MHz, D_2O) δ = 66.80, 52.76, 28.27, 28.10, 25.39, 22.24.

Synthesis of 1,8-Octanebis(trimethylammonium) dibromide (8-Br). Trimethylamine (30% in ethanol, 2.709 g) and 1,8-dibromooctane (1.496 g, 5.5 mmol) were added in a 100 mL round-bottom flask containing 30 mL of methanol. The mixture underwent vigorous stirring at 35 °C for 48 h. Subsequently, a large amount of diethyl ether was added to precipitate the crude product, which was then collected by filtration. The resulting white precipitate was washed three times with 20 mL of acetone followed by 20 mL of diethyl ether, and then dried under vacuum at 40 °C for 12 h. The dried solids were dissolved in methanol and recrystallized using vapor diffusion in a methanol-diethyl ether system. Then the recrystallized products were further purified using a C18 column, followed by a freeze-drying process to obtain the final solid in a yield of 63.4%. ^{1}H NMR (500 MHz, D_2O, ppm) δ = 3.36 – 3.30 (m, 4H), 3.12 (s, 18H), 1.85 – 1.75 (m, 4H), 1.40 (s, 8H). ^{13}C NMR (126 MHz, D_2O) δ = 66.73, 52.83, 27.91, 25.29, 22.23.

Synthesis of 1,10-Decanebis(trimethylammonium) diiodide (10-I). Trimethylamine (30% in ethanol, 2.463 g) and 1,10-diiododecane (1.970 g, 5.0 mmol) were added in a 100 mL round-bottom flask containing 30 mL of methanol. The mixture underwent vigorous stirring at 25 °C for 72 h under protection from light. Subsequently, a large amount of diethyl ether was added to precipitate the crude product, which was then collected by filtration. The resulting white precipitate was washed three times with 20 mL of acetone followed by 20 mL of diethyl ether, and then dried under vacuum at 25 °C for 16 h. The dried solids were dissolved in methanol and recrystallized using vapor diffusion in a methanol-diethyl ether system. Then the recrystallized products were further purified using a C18 column, followed by a freeze-drying process to obtain the final solid in a yield of 58.6%. ^{1}H NMR (500 MHz, D_2O, ppm) δ = 3.35 – 3.28 (m, 4H), 3.10 (s, 18H), 1.85 – 1.72 (m, 4H), 1.34 (d, *J* = 16.9 Hz, 12H). ^{13}C NMR (126 MHz, D_2O) δ = 66.80, 52.88, 28.27, 28.10, 25.40, 22.27.

Single-crystal cultivation. 10-Br-a was obtained by slow evaporation of its ethanol-water solution, and 10-Br-b was obtained by slow cooling of its saturated acetonitrile solution. 8-Br-a was acquired through slow evaporation of its ethanol aqueous solution, and 8-Br-b was acquired through slow vapor diffusion in a methanol-diethyl ether system. 10-I-MeCN, 10-I-MeOH and 10-I-H_2O were gained through slow cooling of saturated solutions of acetonitrile, methanol and water, respectively.

Supplementary Figures and Tables

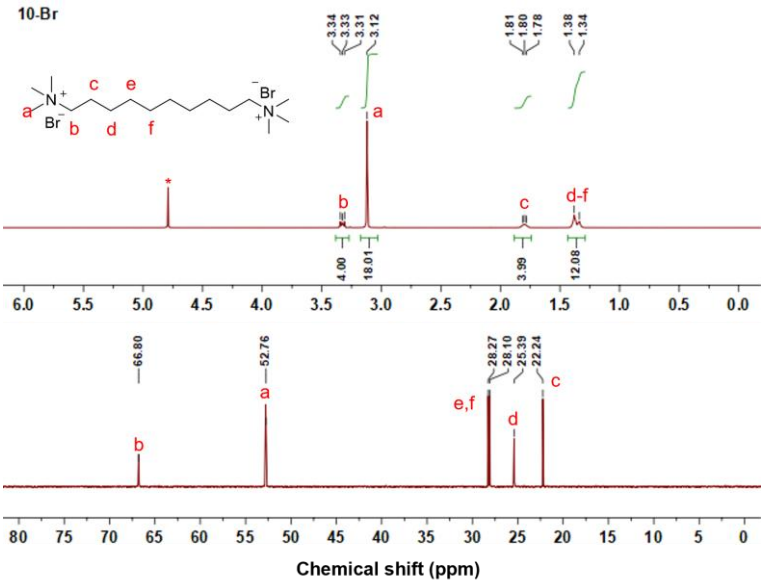

Fig. S1 ^{1}H and ^{13}C NMR spectra of 10-Br in D_2O

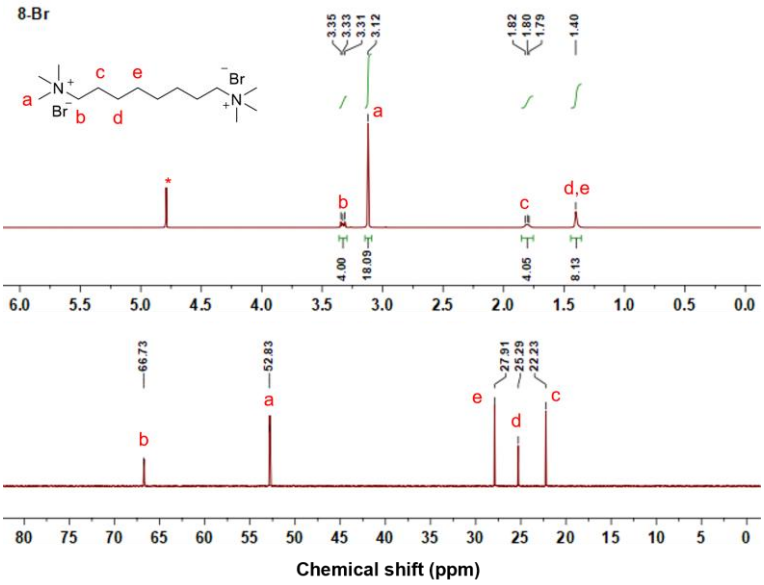

Fig. S2 ^{1}H and ^{13}C NMR spectra of 8-Br in D_2O.

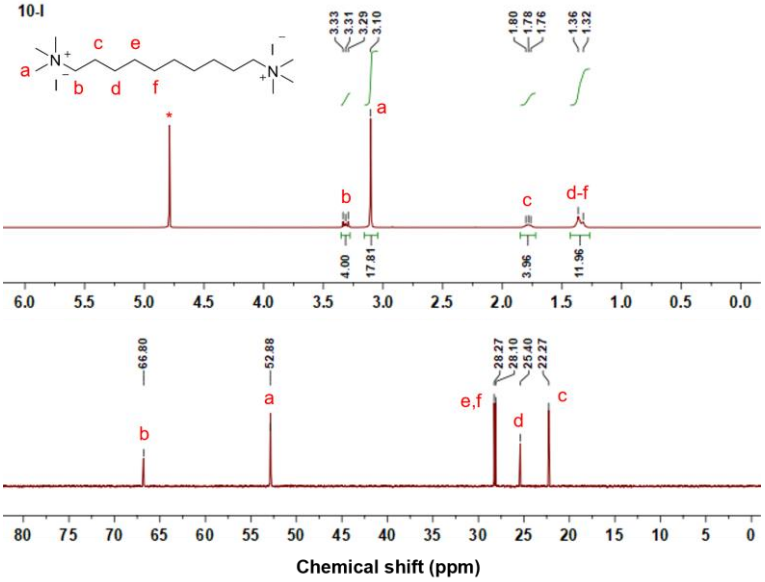

Fig. S3 ^{1}H and ^{13}C NMR spectra of 10-I in D_2O.

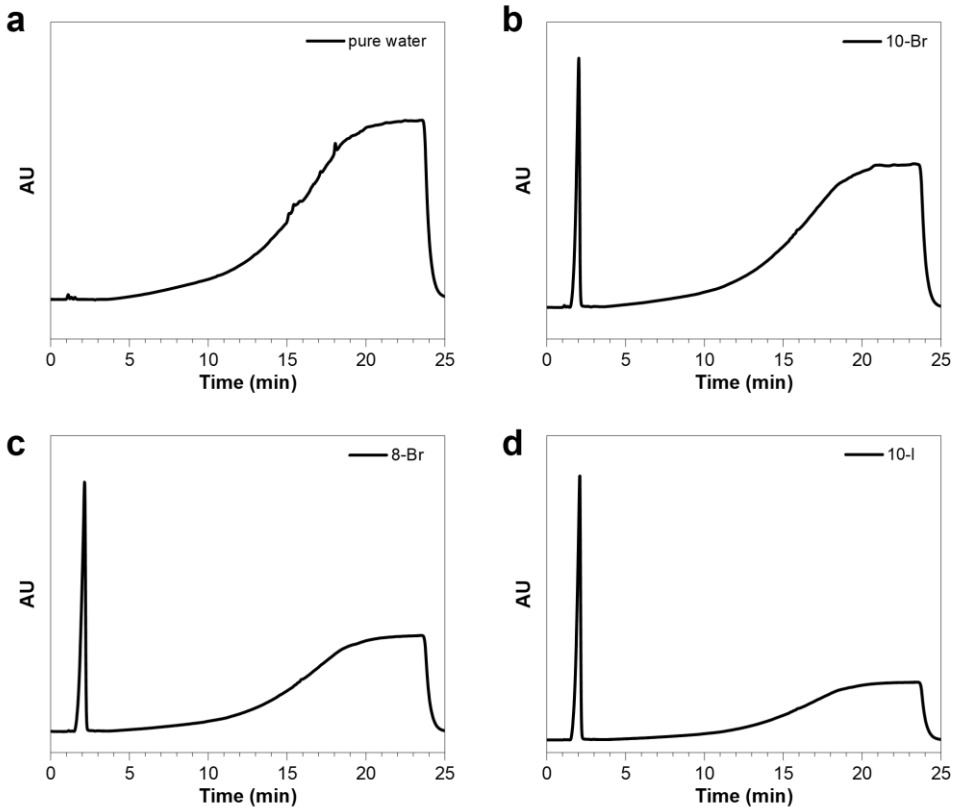

Fig. S4 The HPLC results of (a) pure water, (b) 10-Br, (c) 8-Br and (d) 10-I compounds.

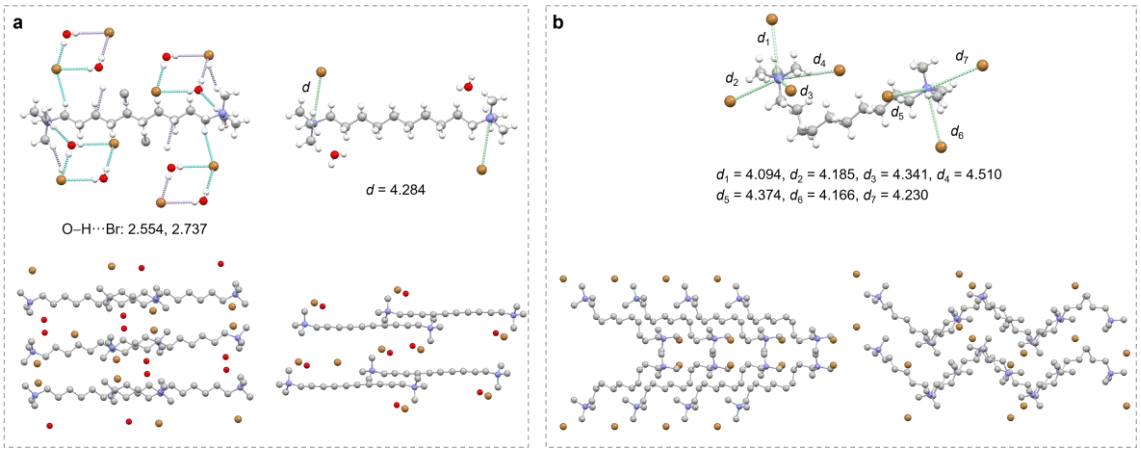

Fig. S5 Single crystal structure and fragmental molecular packing of (a) 10-Br-a and (b) 10-Br-b.

Table S1. Single crystal data of two10-Br polymorphs.

	10-Br-a	10-Br-b
Formula	$C_{16}H_{38}Br_2N_2{\cdot}2(H_2O)$	$C_{16}H_{38}Br_2N_2$
Formula weight	454.32	418.28
Wavelength (Å)	1.54178	1.54184
Space group	P21/c	Pbca
Cell length (Å)	a=9.060 (4) b=10.028 (5) c=13.559 (6)	a=11.9427 (2) b=11.6291 (2) c=28.3098 (4)
Cell angle (°)	α=90 β=109.52 γ=90	α=90 β=90 γ=90
Cell volume (Å^3)	1161.1(9)	3931.75(11)
Z	2	8
Density (g·cm^{-3})	1.299	1.413
F (000)	476.0	1744.0
h_{max}, k_{max}, l_{max}	10, 12, 16	14, 14, 35
T_{min}, T_{max}	0.513, 0.584	0.459, 0.538

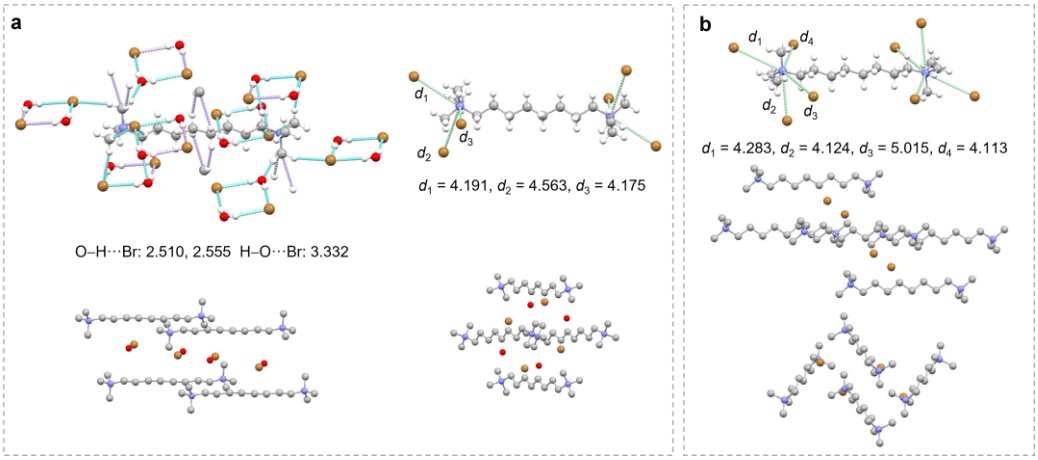

Fig. S6 Single crystal structure and fragmental molecular packing of (a) 8-Br-a and (b) 8-Br-b.

Table S2. Single crystal data of two 8-Br polymorphs.

	8-Br-a	8-Br-b
Formula	$C_{14}H_{34}Br_2N_2{\cdot}2(H_2O)$	$C_{14}H_{34}Br_2N_2$
Formula weight	426.26	390.23
Wavelength (Å)	1.54184	1.54184
Space group	P21/n	P21/n
Cell length (Å)	a=7.9725 (3) b=10.1116 (2) c=12.9668 (3)	a=5.8652 (1) b=12.0120 (2) c=13.5766 (2)
Cell angle (°)	α=90 β=103.377(3) γ=90	α=90 β=98.999(2) γ=90
Cell volume (Å^3)	1161.96(5)	944.74(3)
Z	2	2
Density (g·cm^{-3})	1.392	1.372
F (000)	444.0	404.0
h_{max}, k_{max}, l_{max}	10, 12, 16	7, 15, 17
T_{min}, T_{max}	0.466, 0.544	0.395, 0.425

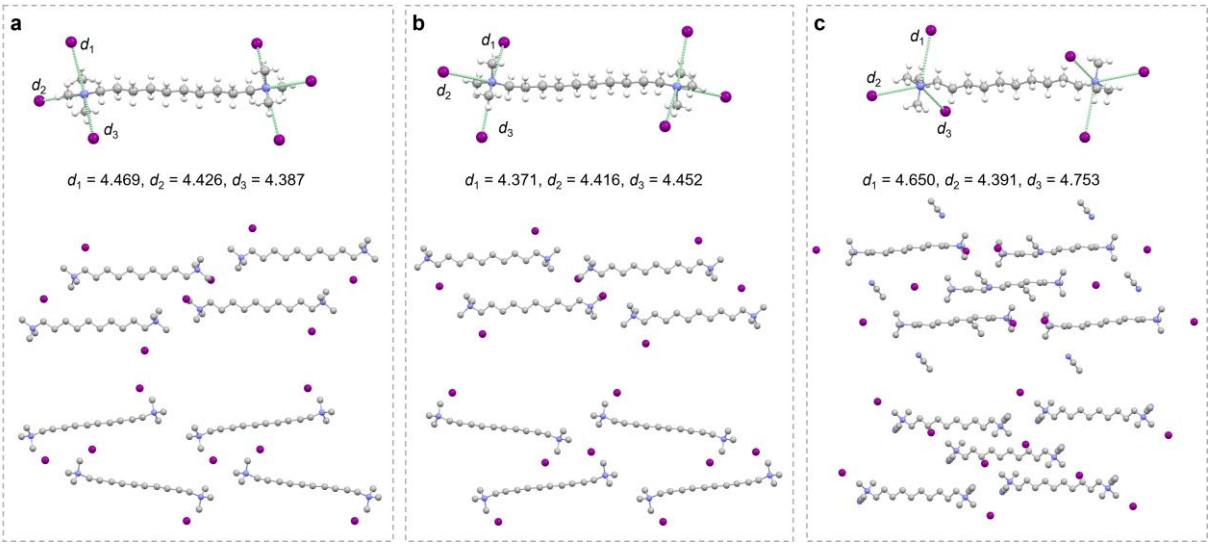

Fig. S7 Single crystal structure and fragmental molecular packing of (a) 10-I-H_2O, (b) 10-I-MeOH and (c) 10-I-MeCN.

Table S3. Single crystal data of three 10-I polymorphs.

	10-I-H_2O	10-I-MeOH	10-I-MeCN
Formula	$C_{16}H_{38}I_2N_2$[+solvent]	$C_{16}H_{38}I_2N_2$[+solvent]	$C_{16}H_{38}I_2N_2 \cdot 2(C_2H_3N)$
Formula weight	512.28	512.28	594.39
Wavelength (Å)	0.71073	0.71073	0.71073
Space group	C2/c	C2/c	P-1
Cell length (Å)	a=18.6422 (8) b=13.4664 (5) c=13.1607 (10)	a=18.646 (3) b=13.3913 (14) c=14.6422 (18)	a=7.1074 (4) b=9.9391 (6) c=10.6725 (7)
Cell angle (°)	α=90 β=128.465(1) γ=90	α=90 β=135.346(3) γ=90	α=66.333(3) β=86.755(2) γ=85.466(2)
Cell volume ($Å^3$)	2586.9(2)	2569.6(6)	688.09(7)
Z	4	4	1
Density ($g \cdot cm^{-3}$)	1.315	1.324	1.434
F (000)	1016.0	1016.0	298.0
h_{max}, k_{max}, l_{max}	32, 23, 23	24, 17, 19	8, 12, 13
T_{min}, T_{max}	0.564, 0.615	0.619, 0.676	0.699, 0.725

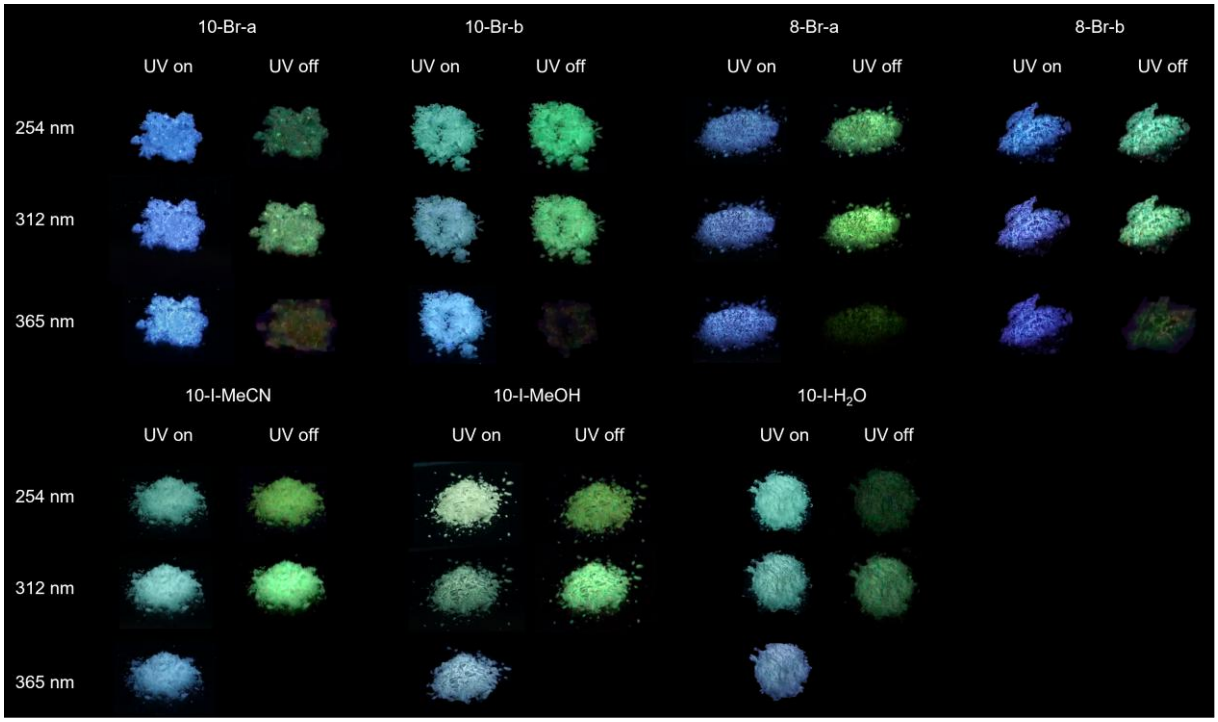

Fig. S8 Luminescent photographs of all GAQAS polymorphs under and after ceasing 254, 312 and 365 nm UV irradiations.

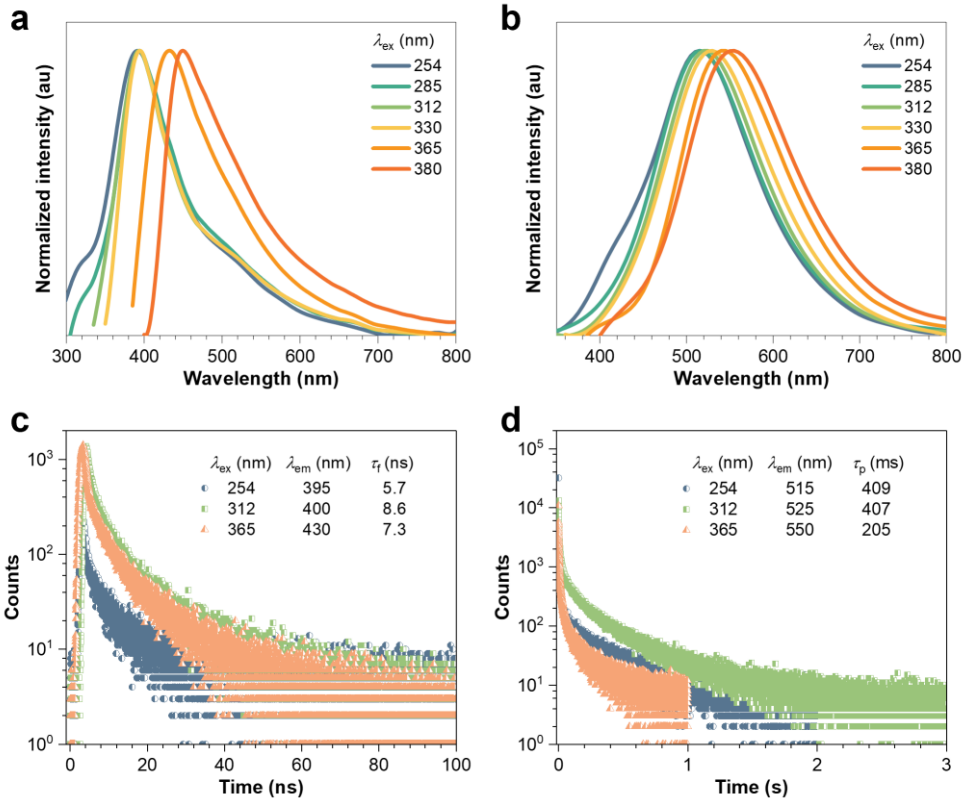

Fig. S9 (a) Prompt and (b) delayed (t_d = 1 ms) emission spectra, (c) fluorescence and (d) phosphorescence lifetimes of 10-Br-a under different excitation wavelengths (λ_{ex}s).

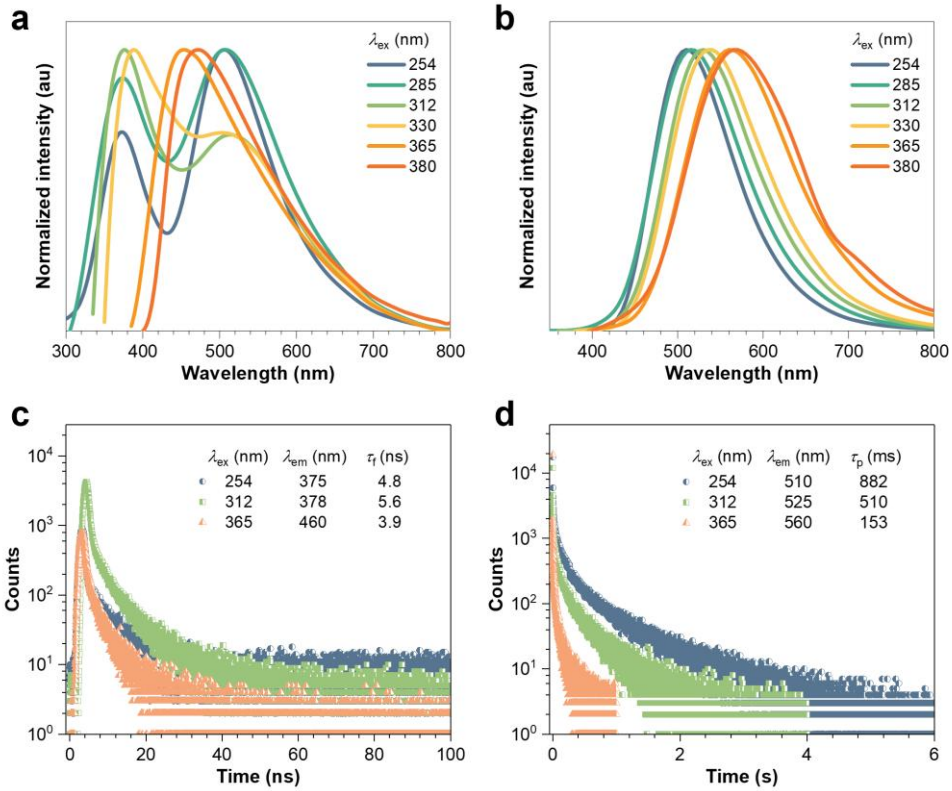

Fig. S10 (a) Prompt and (b) delayed (t_d = 1 ms) emission spectra, (c) fluorescence and (d) phosphorescence lifetimes of 10-Br-b under different λ_{ex}s.

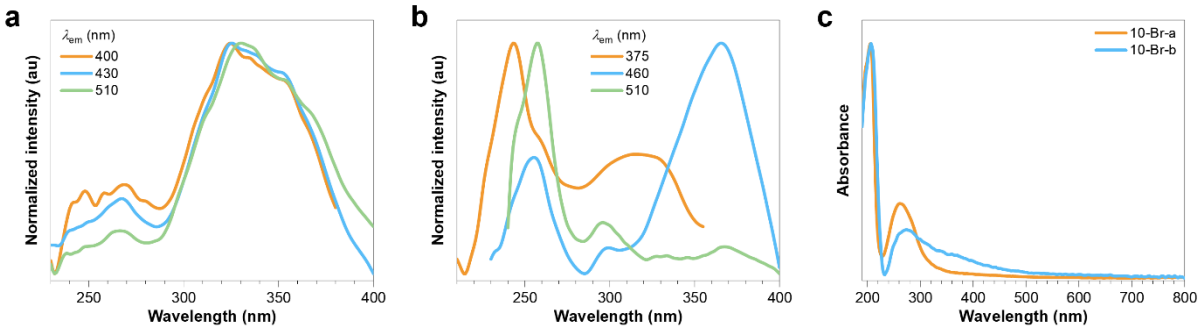

Fig. S11 Excitation spectra of (a) 10-Br-a and (b)10-Br-b measured at different emission wavelengths (λ_{em}s). (c) Absorption spectra of 10-Br polymorphs.

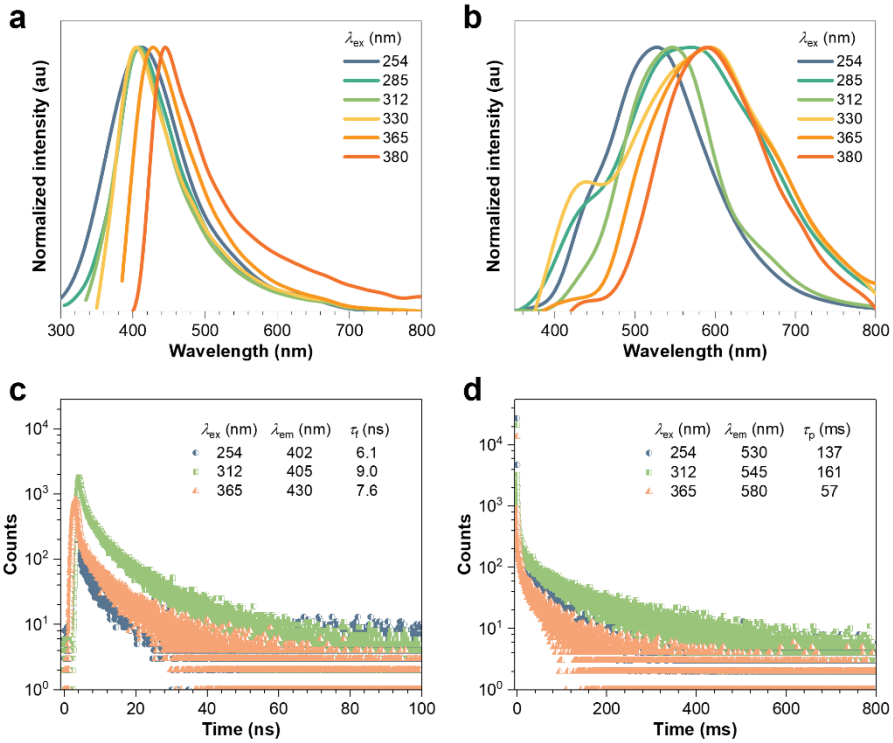

Fig. S12 (a) Prompt and (b) delayed (t_d = 1 ms) emission spectra, (c) fluorescence and (d) phosphorescence lifetimes of 8-Br-a under different λ_{ex}s.

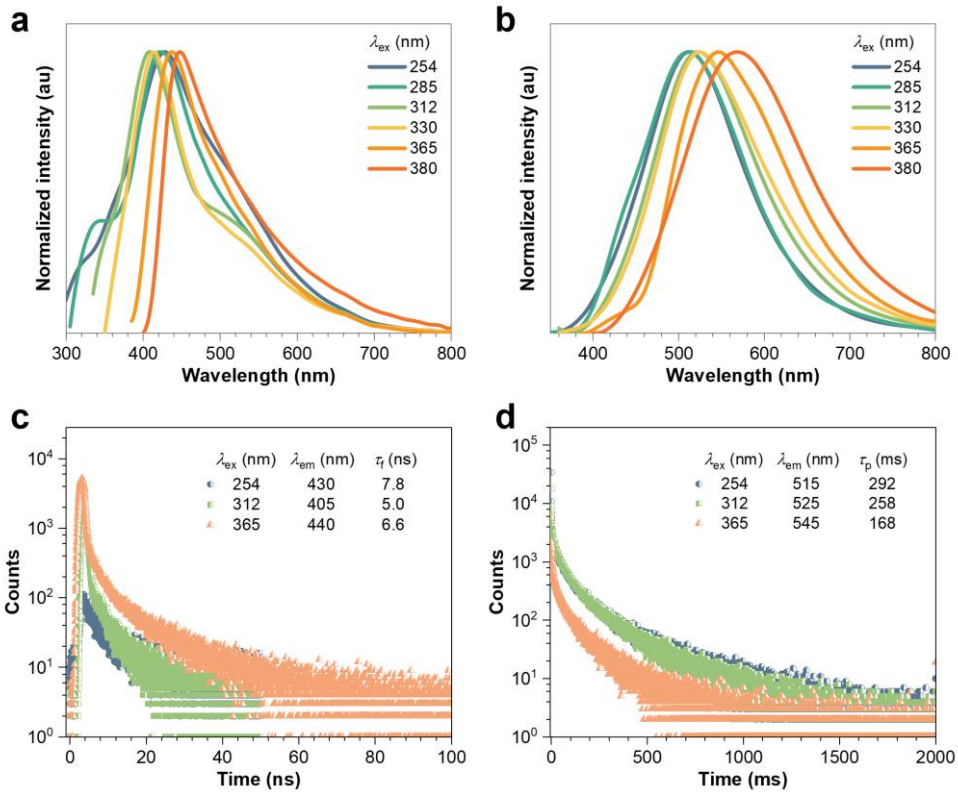

Fig. S13 (a) Prompt and (b) delayed (t_d = 1 ms) emission spectra, (c) fluorescence and (d) phosphorescence lifetimes of 8-Br-b under different λ_{ex}s.

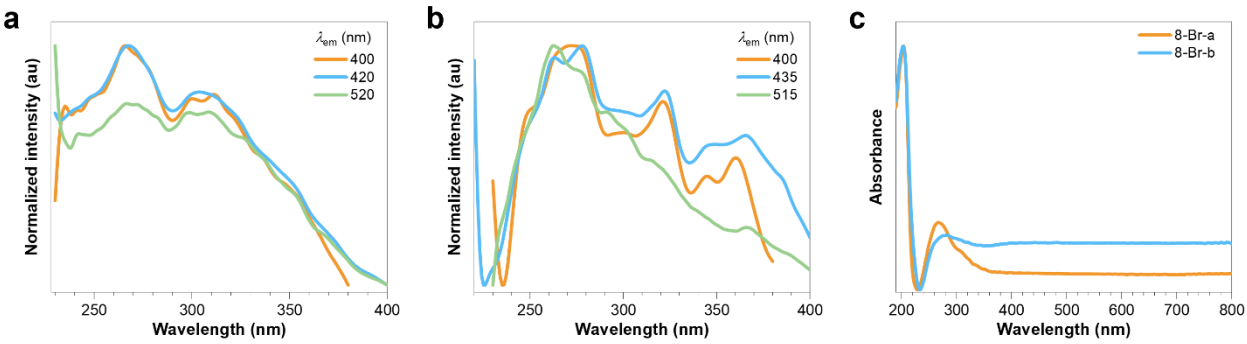

Fig. S14 Excitation spectra of (a) 8-Br-a and (b) 8-Br-b measured at different λ_{em}s. (c) Absorption spectra of 8-Br polymorphs.

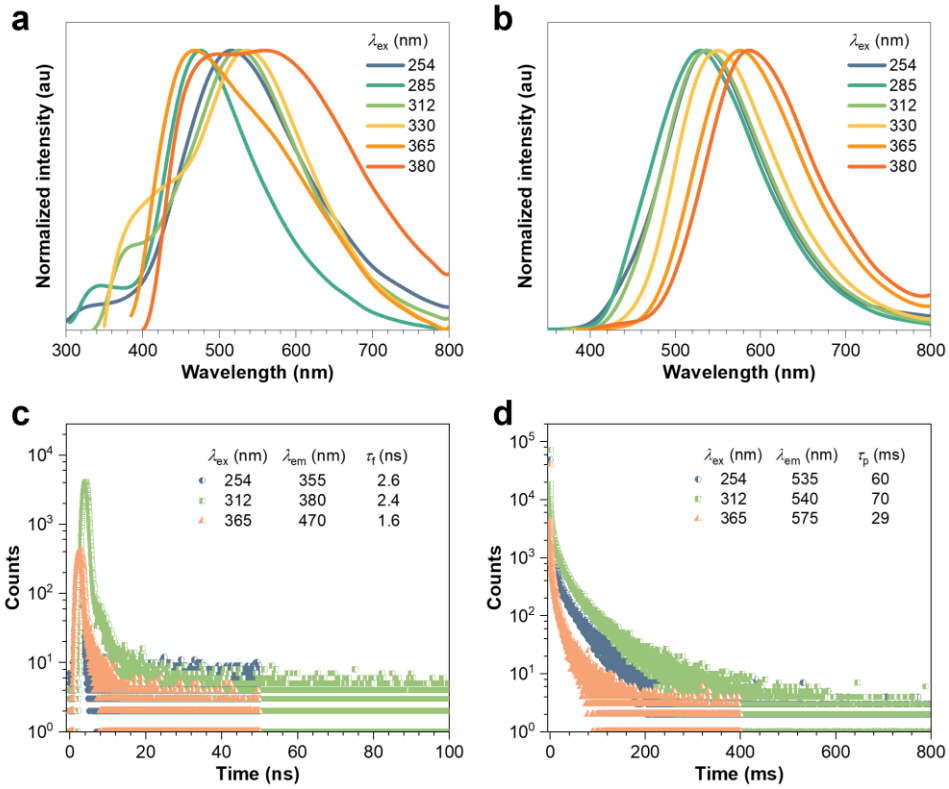

Fig. S15 (a) Prompt and (b) delayed (t_d = 1 ms) emission spectra, (c) fluorescence and (d) phosphorescence lifetimes of 10-I-H_2O under different λ_{ex}s.

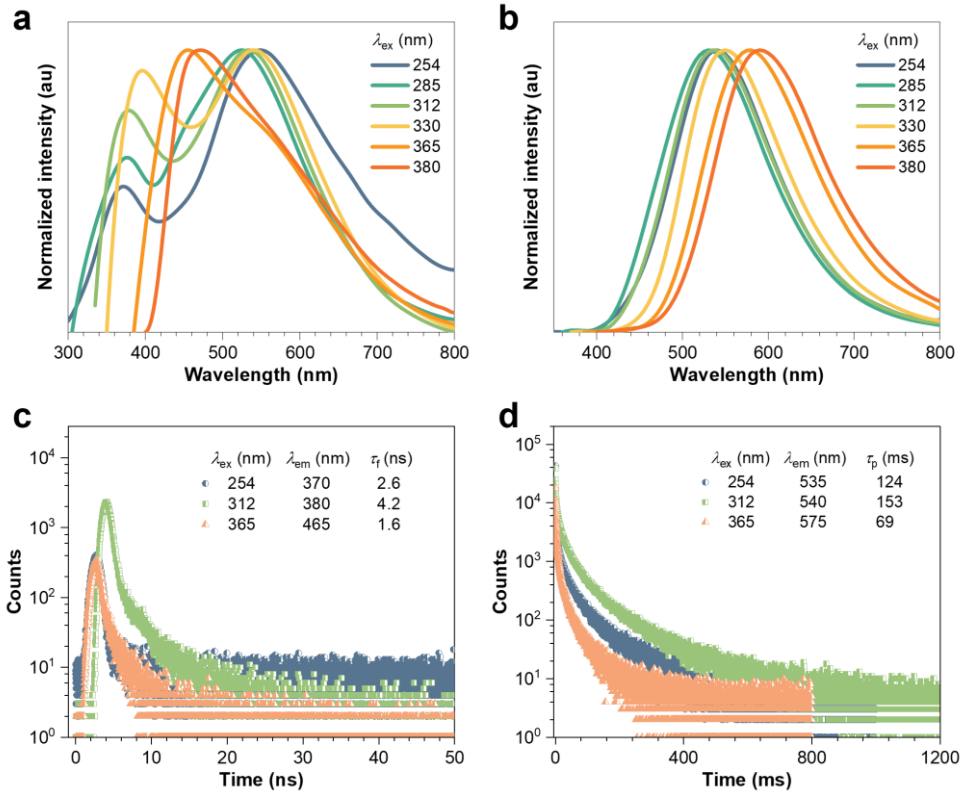

Fig. S16 (a) Prompt and (b) delayed (t_d = 1 ms) emission spectra, (c) fluorescence and (d) phosphorescence lifetimes of 10-I-MeOH under different λ_{ex}s.

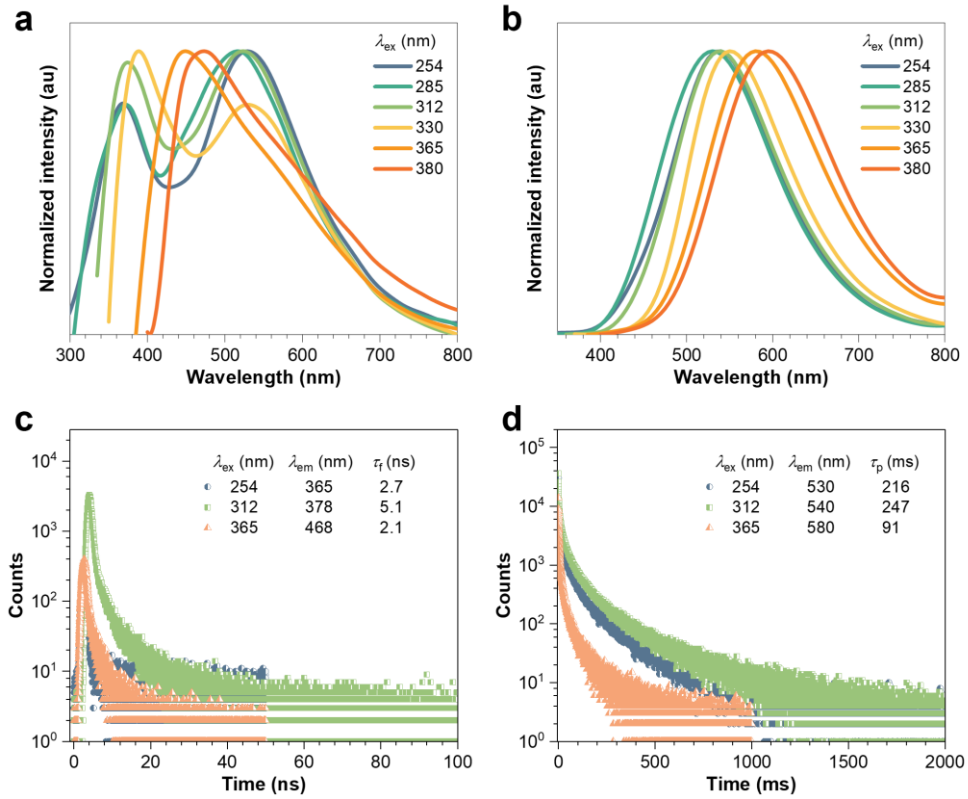

Fig. S17 (a) Prompt and (b) delayed (t_d = 1 ms) emission spectra, (c) fluorescence and (d) phosphorescence lifetimes of 10-I-MeCN under different λ_{ex}s.

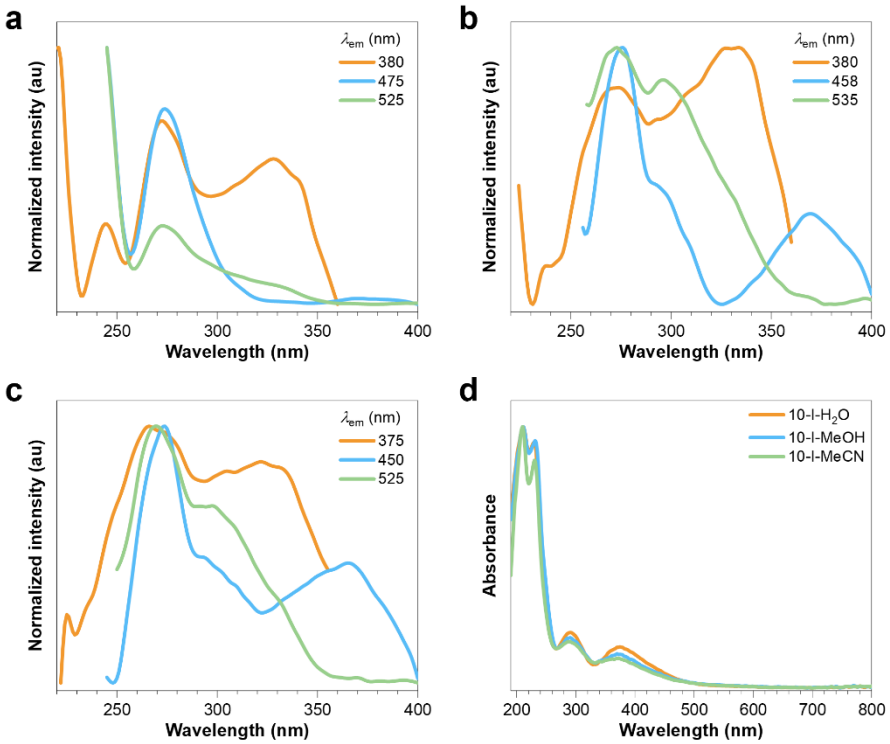

Fig. S18 Excitation spectra of (a) 10-I-H_2O, (b) 10-I-MeOH and (c) 10-I-MeCN measured at different λ_{em}s. (d) Absorption spectra of 10-I polymorphs.

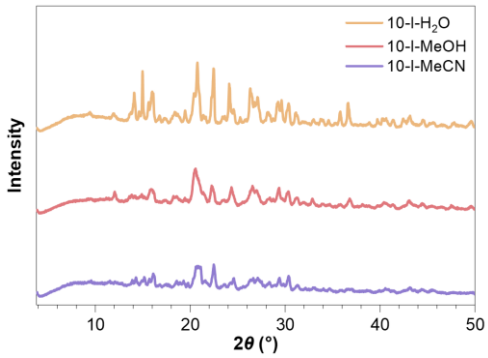

Fig. S19 XRD patterns of three 10-I polymorphs.

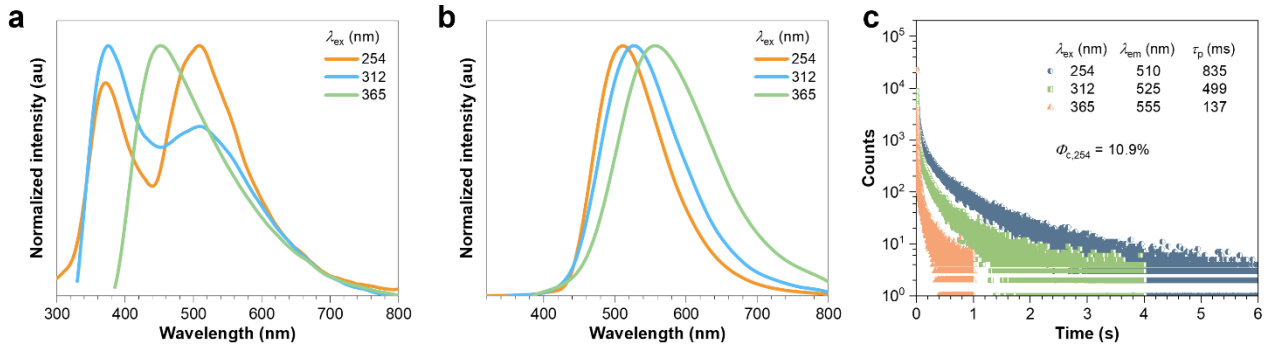

Fig. S20 (a) Prompt and (b) delayed emission spectra and (c) phosphorescence lifetimes of 10-Br-b under different λ_{ex}s after being stored for six months. The crystal efficiency is also given in (c).

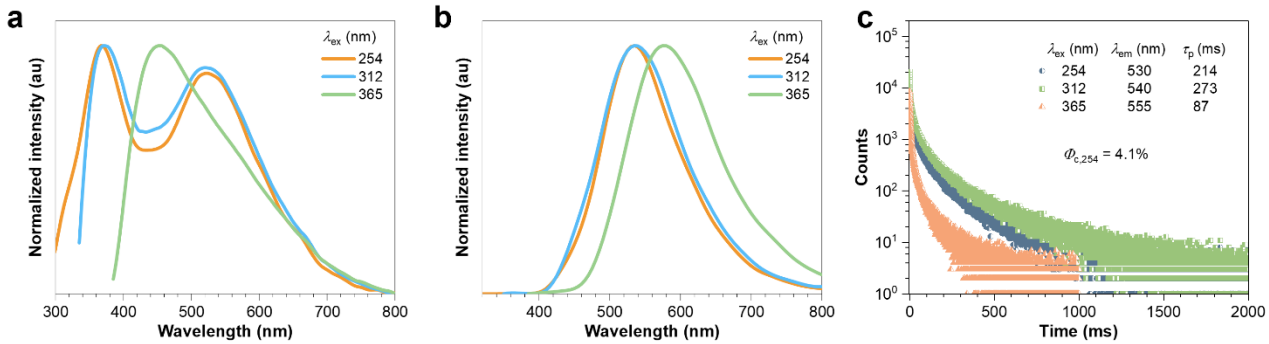

Fig. S21 (a) Prompt and (b) delayed emission spectra and (c) phosphorescence lifetimes of 10-I-MeCN under different λ_{ex}s after being stored for six months. The crystal efficiency is also given in (c).

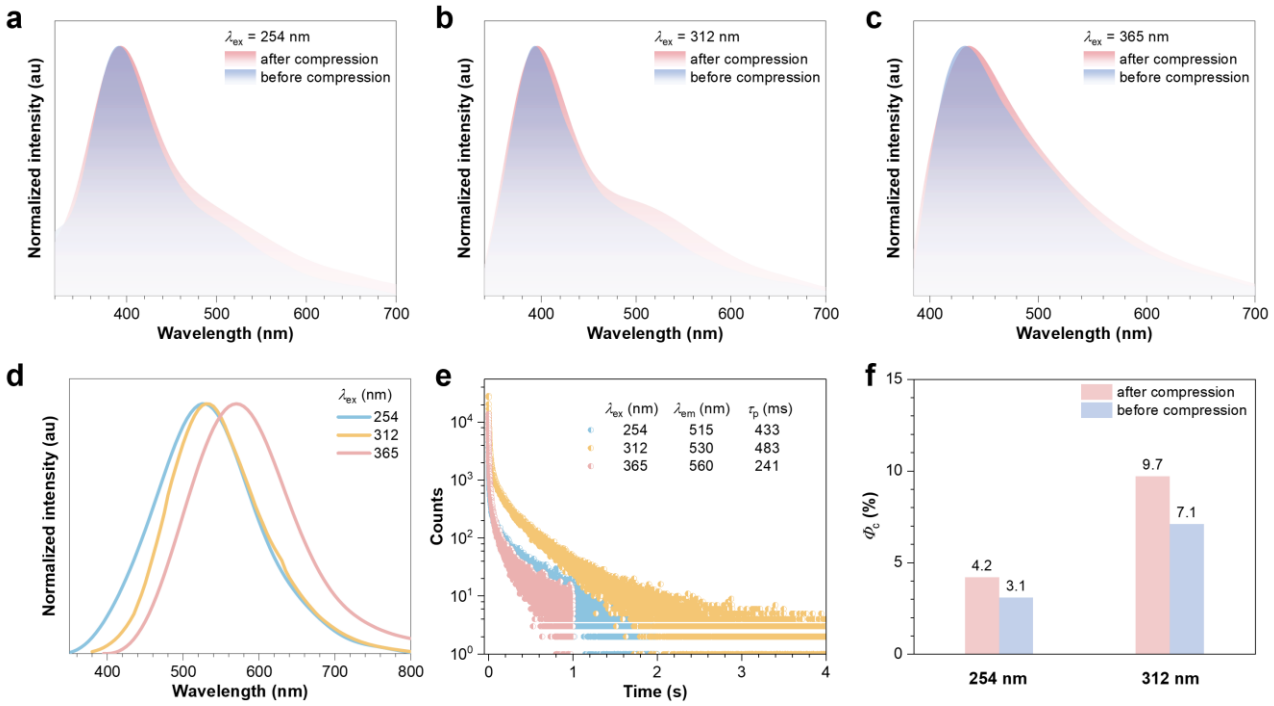

Fig. S22 Prompt emission spectra of 10-Br-a before and after compression under (a) 254, (b) 312 and (c) 365 nm UV irradiation. (d) Delayed (t_d = 1 ms) emission spectra and (e) phosphorescence lifetimes of 10-Br-a after compression under different λ_{ex}s. (f) Total quantum yields of 10-Br-a before and after compression under 254 and 312 nm UV irradiations.

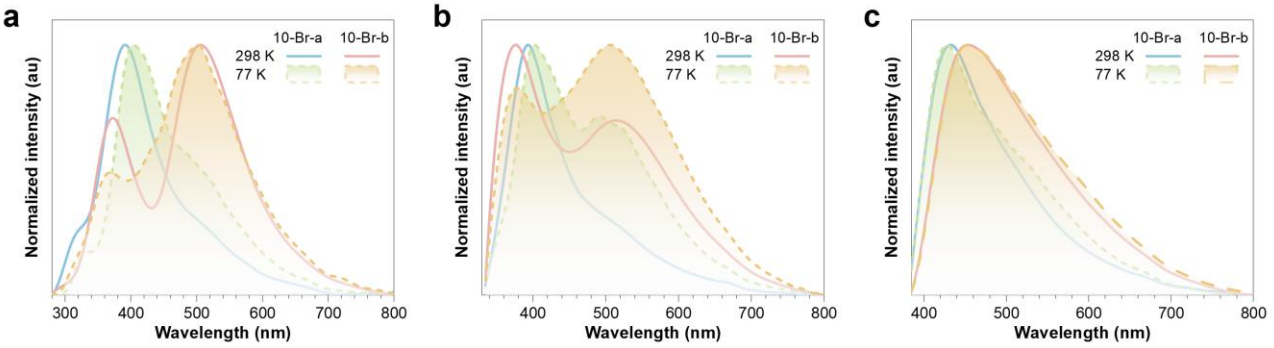

Fig. S23 Prompt emission spectra of 10-Br-a and 10-Br-b at room temperature and 77 K under (a) 254, (b) 312 and (c) 365 nm UV irradiations.

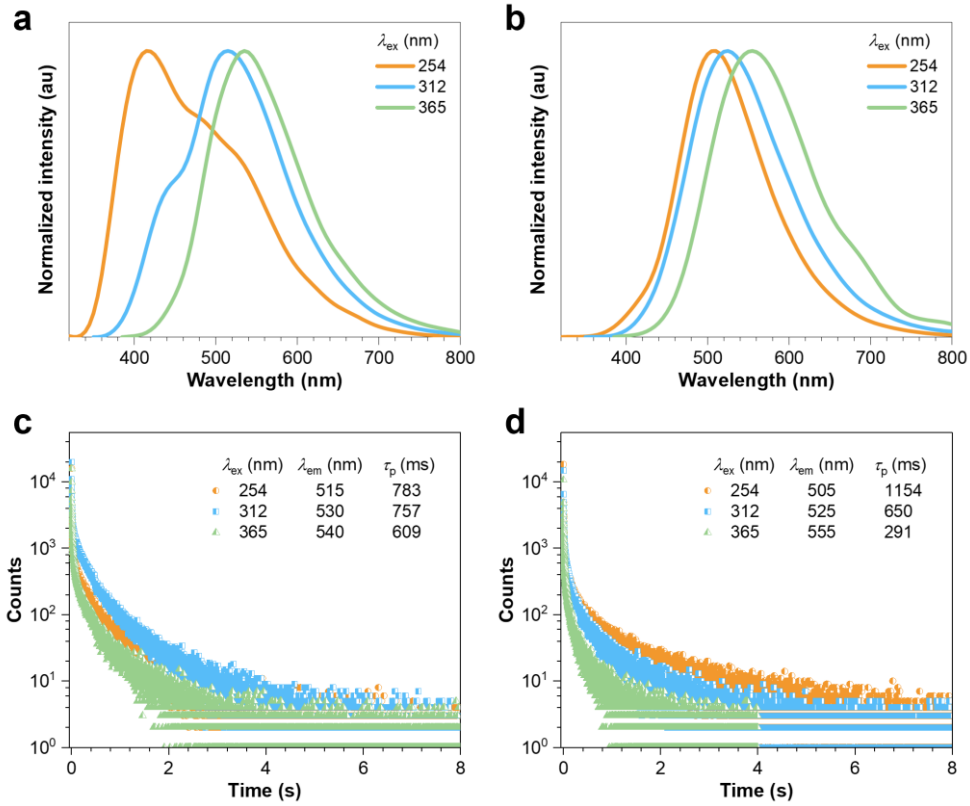

Fig. S24 (a,b) Delayed (t_d = 1 ms) emission spectra and (c,d) phosphorescence lifetimes of (a,c) 10-Br-a and (b,d) 10-Br-b at 77 K under different λ_{ex}s.

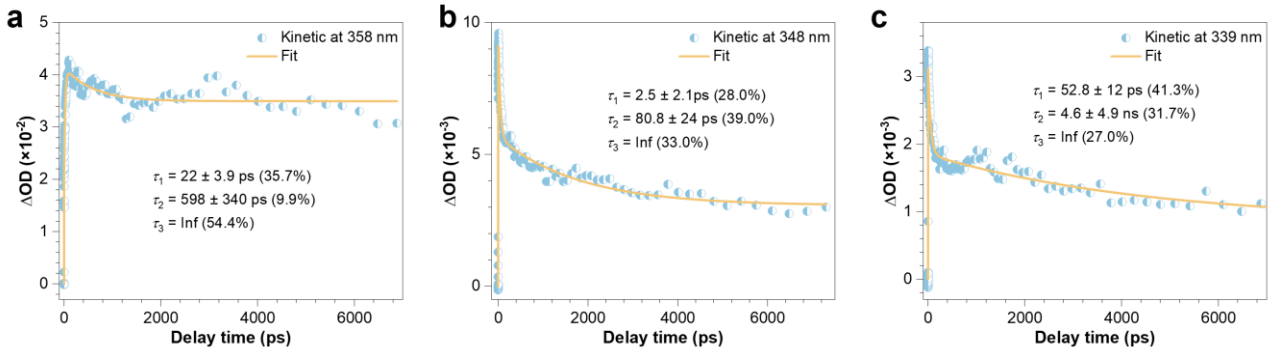

Fig. S25 The fs-TA spectra decay curve of (a) 10-Br aqueous solution (2 M), (b) 10-Br-a polymorphic powder and (c) 10-Br-b polymorphic powder with peaks at 358, 348 and 339 nm, respectively.

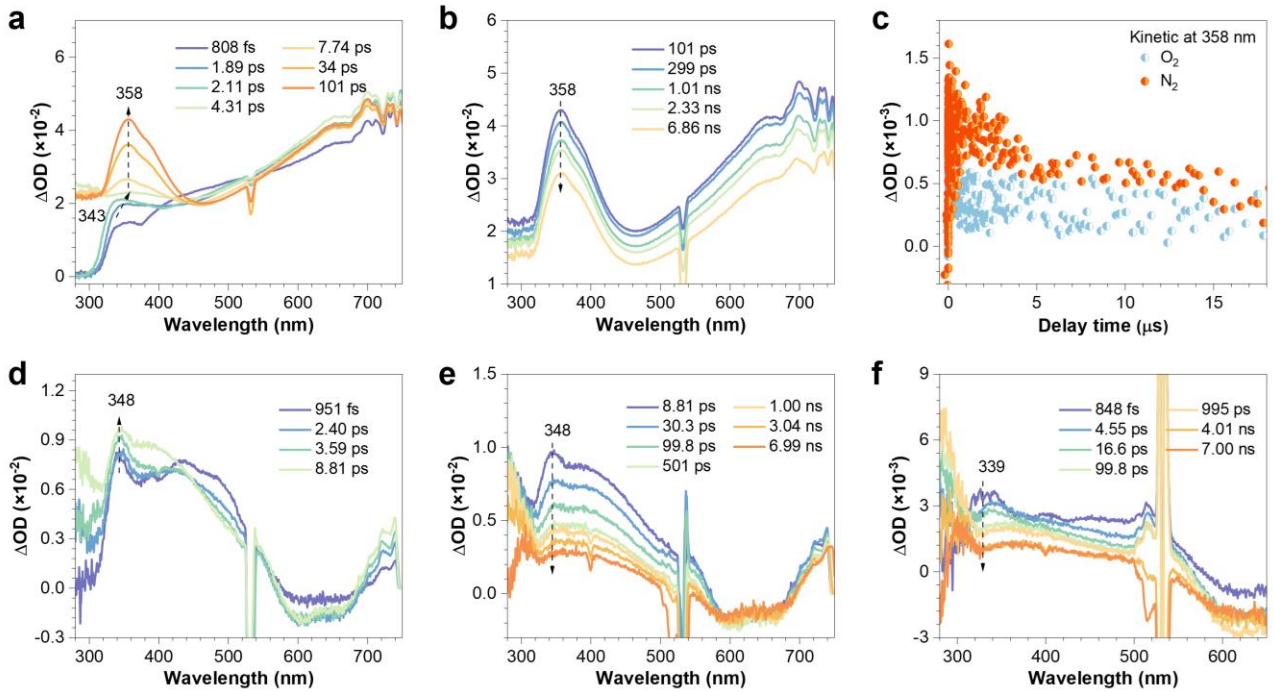

Fig. S26 (a,b) fs-TA spectra of 10-Br aqueous solution (2 M) after 266 nm UV excitation. (c) ns-TA spectra decay curve of 10-Br aqueous solution under N_2 and O_2 atmosphere. fs-TA spectra of (d,e) 10-Br-a and (f) 10-Br-b polymorphic powders after 266 nm UV irradiation. ***Note*:** The λ_{ex} of the ultrafast spectroscopy at 266 nm generates a second harmonic peak at 532 nm. For clarity, Fig. 4 in the manuscript presents the ultrafast spectra without second harmonic peaks. To ensure data completeness, the whole ultrafast spectra are provided in Fig. S24.

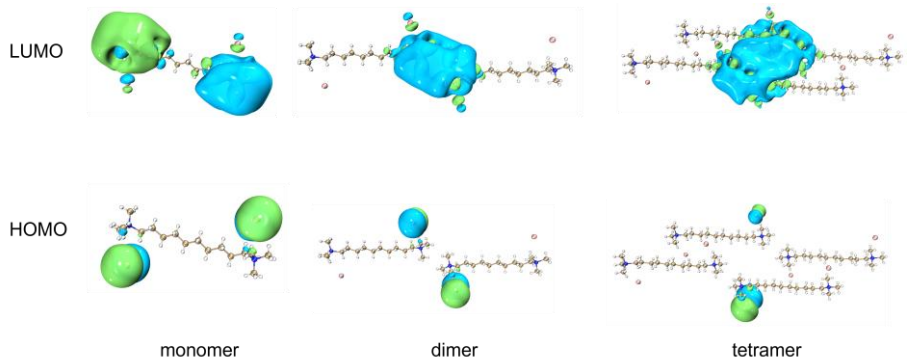

Fig. S27 Electron density distributions of the HOMO and LUMO levels of 10-Br-a.

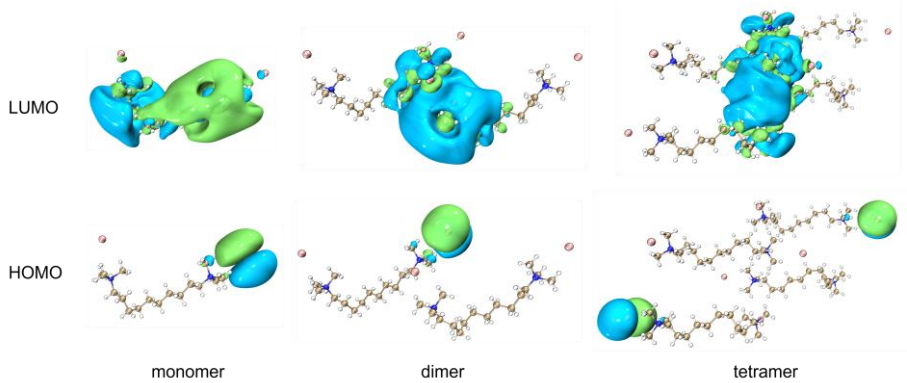

Fig. S28 Electron density distributions of the HOMO and LUMO levels of 10-Br-b.

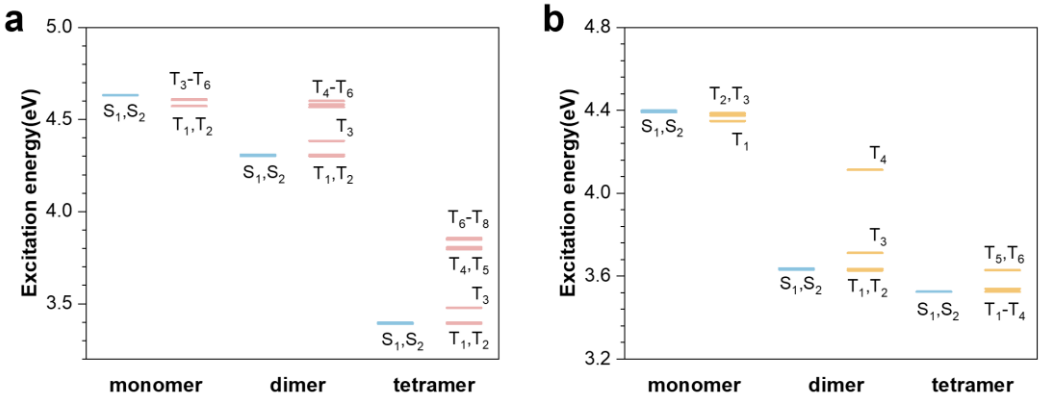

Fig. S29 Excitation energy diagrams of (a) 10-Br-a and (b) 10-Br-b.

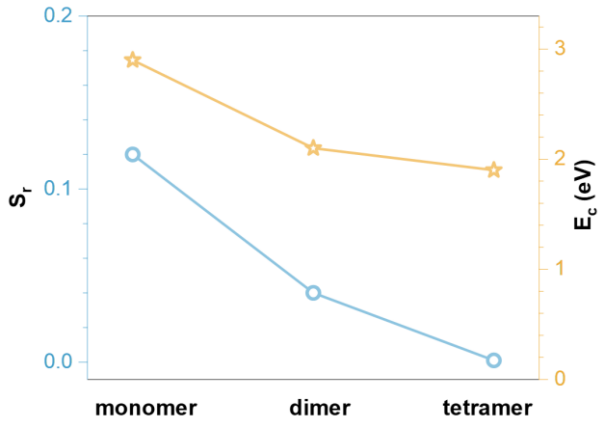

Fig. S30 S_r and E_c values of 10-Br-b from monomer to tetramer.

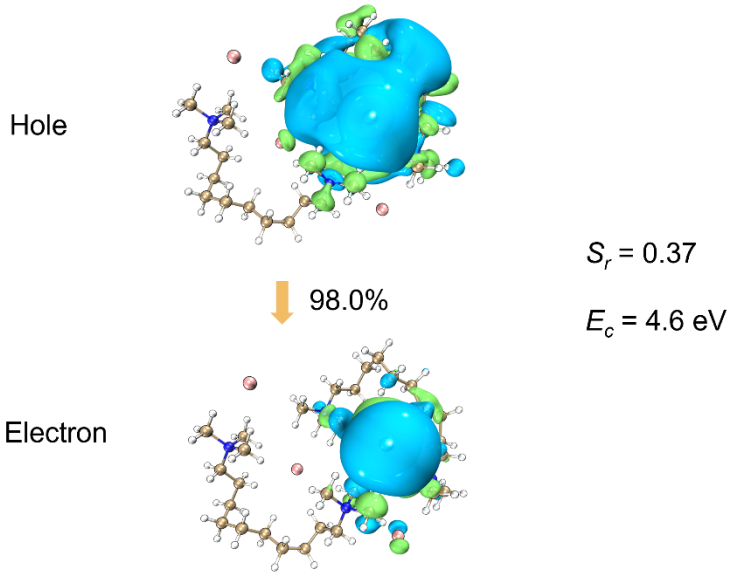

Fig. S31 The NTOs and corresponding *Sr* and *Ec* values for optimized 10-Br-b dimer.

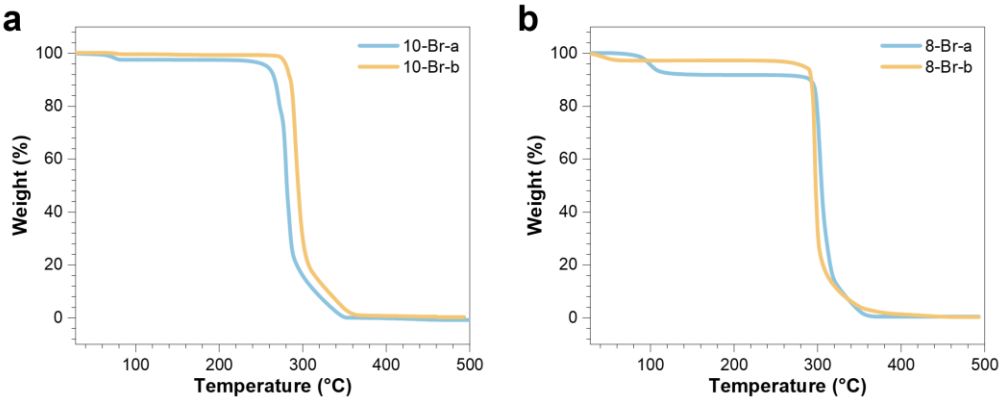

Fig. S32 Thermogravimetry analysis of (a) 10-Br and (b) 8-Br polymorphs (ramp rates = 10 °C min^{-1}).

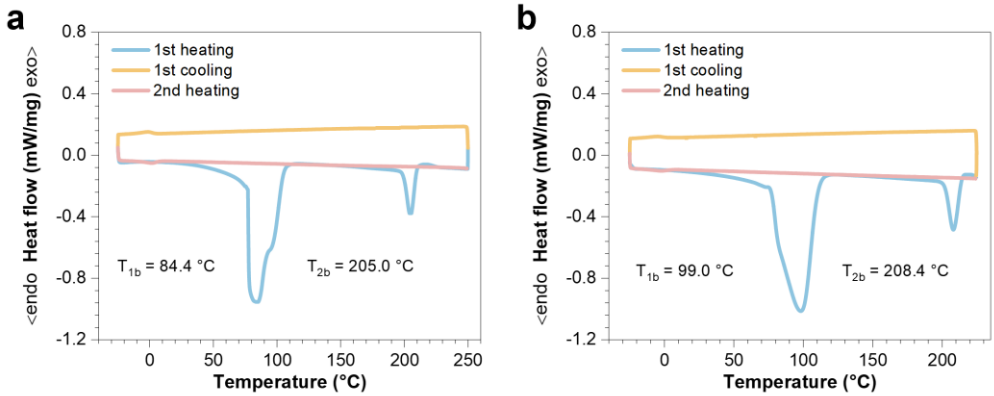

Fig.S33 DSC curves of (a) 8-Br-a and (b) 8-Br-b (ramp rates = 5 °C min^{-1}).

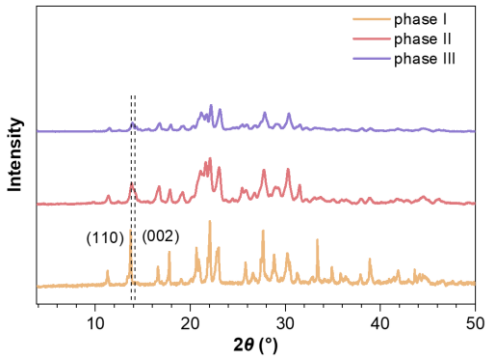

Fig. S34 XRD patterns of different polymorphic phases of 10-Br-a.

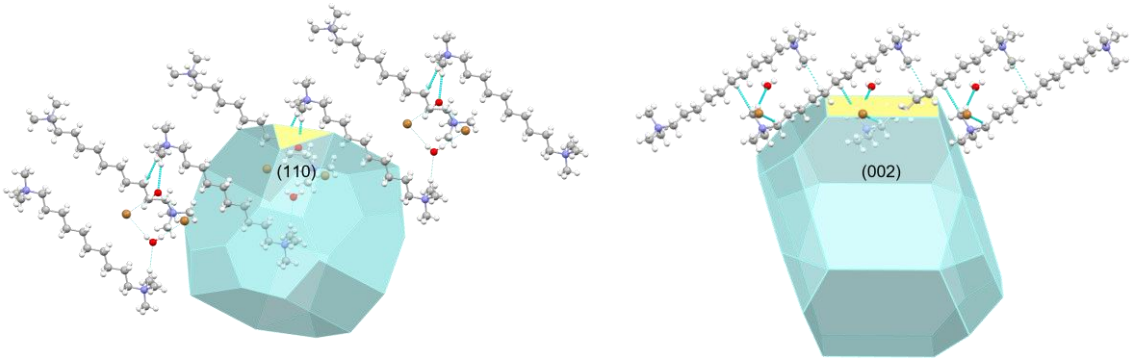

Fig. S35 Predicted crystal morphology and intermolecular interactions of 10-Br-a corresponding to the (110) and (002) planes.

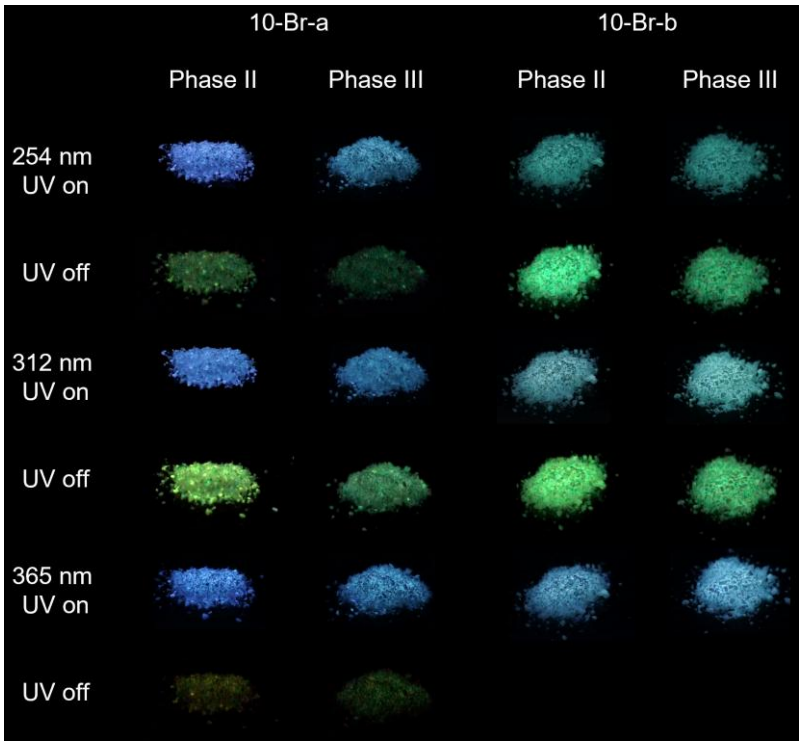

Fig. S36 Luminescent photographs of different 10-Br polymorphic phases under and after different λ_{ex}s.

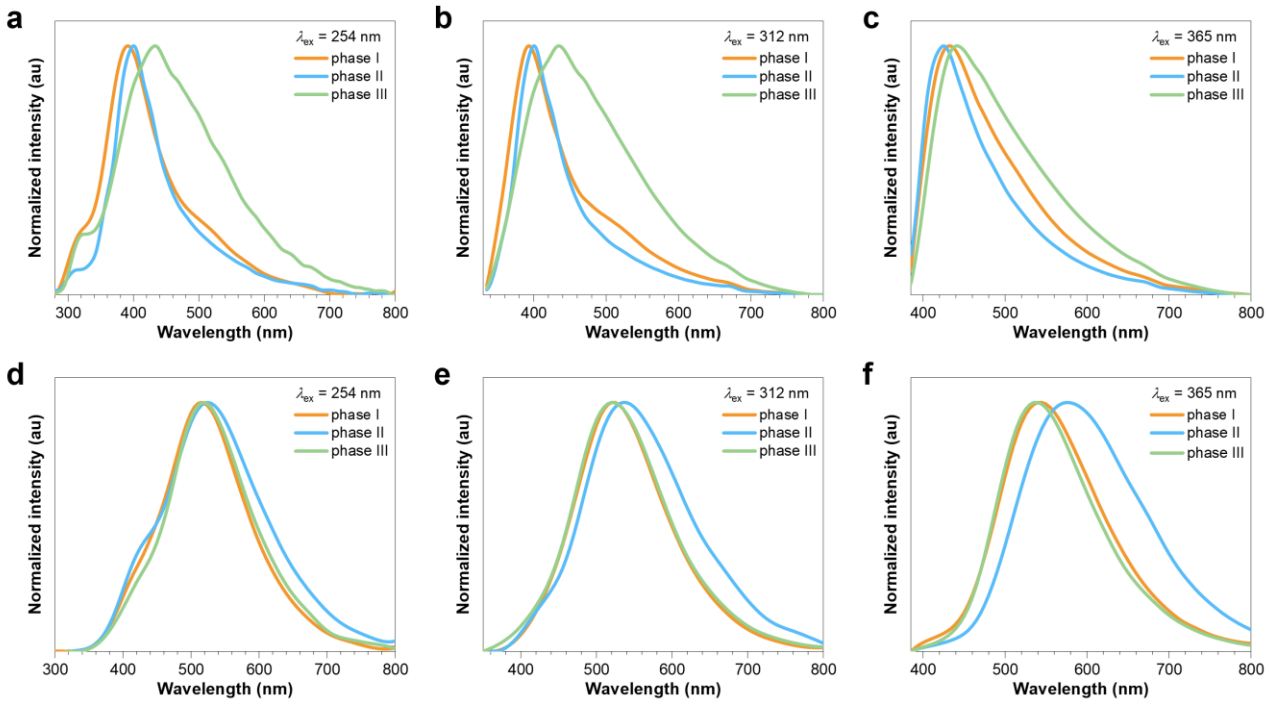

Fig. S37 (a-c) Prompt and (d-f) delayed (t_d = 1 ms) emission spectra of different 10-Br-a polymorphic phases under (a,d) 254, (b,e) 312 and (c,f) 365 nm UV irradiations.

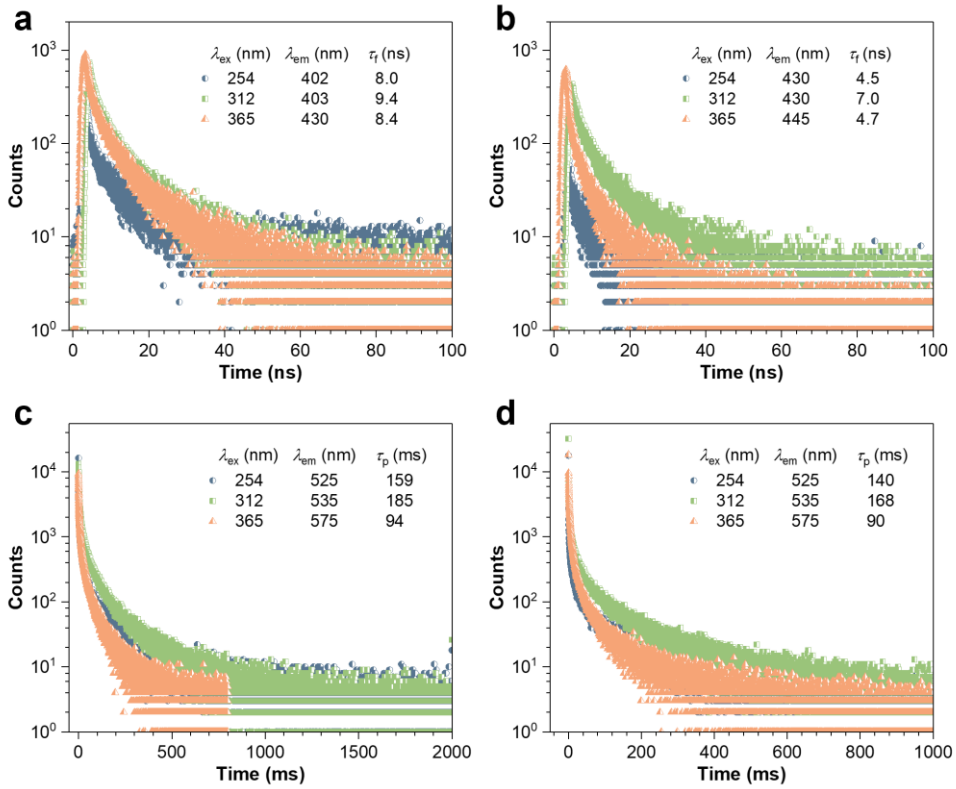

Fig. S38 (a,b) Fluorescence and (c,d) phosphorescence lifetimes of 10-Br-a polymorphic phase (a,c) II and (b,d) III under different λ_{ex}s.

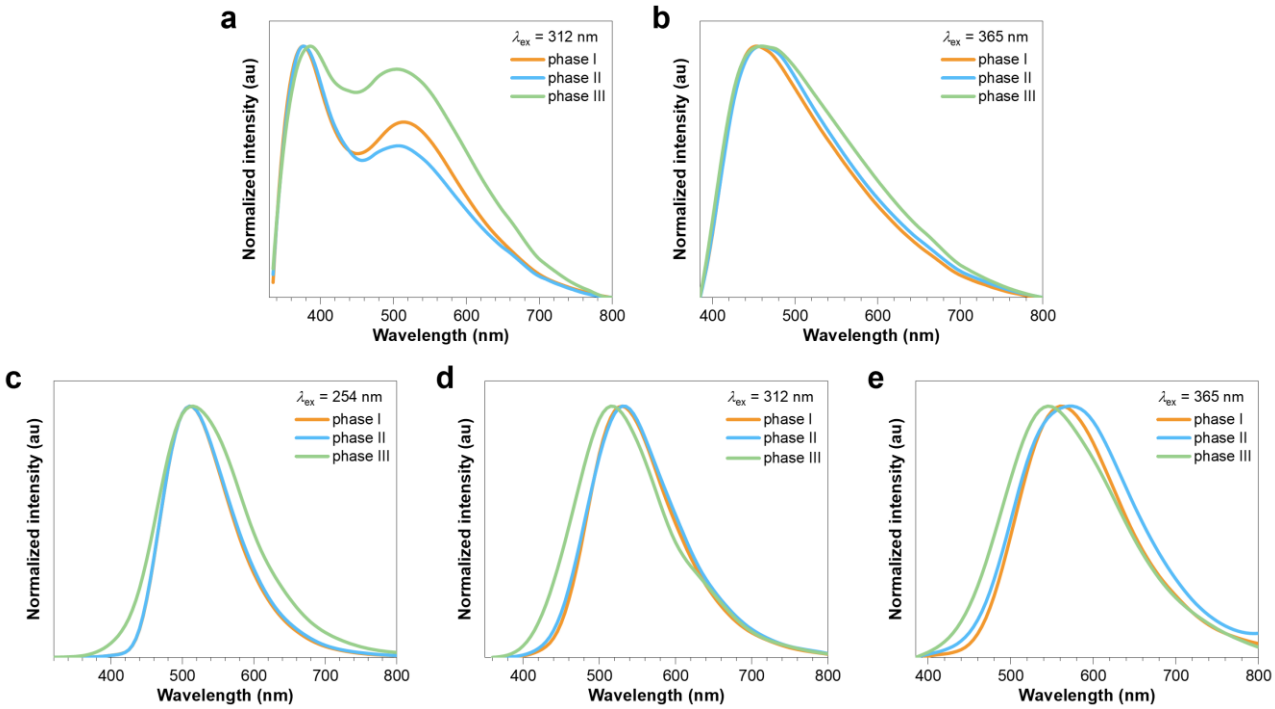

Fig. S39 (a,b) Prompt and (c-e) delayed (t_d = 1 ms) emission spectra of different 10-Br-b polymorphic phases under (c) 254, (a,d) 312 and (b,e) 365 nm UV irradiations.

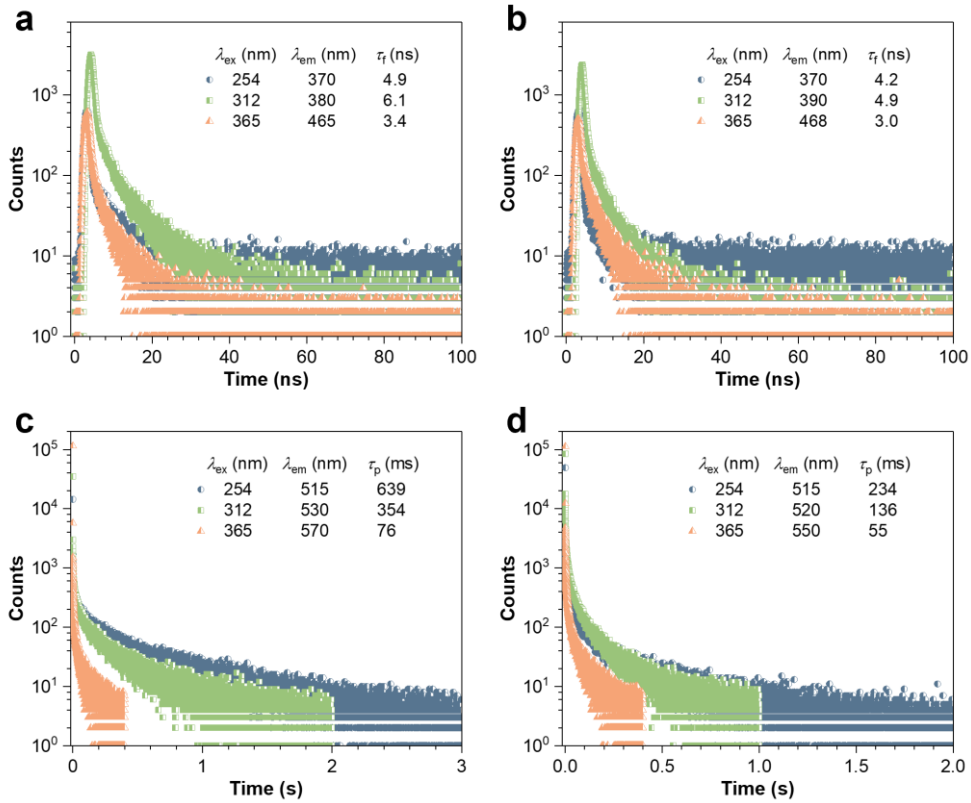

Fig. S40 (a,b) Fluorescence and (c,d) phosphorescence lifetimes of 10-Br-b polymorphic phase (a,c) II and (b,d) III.

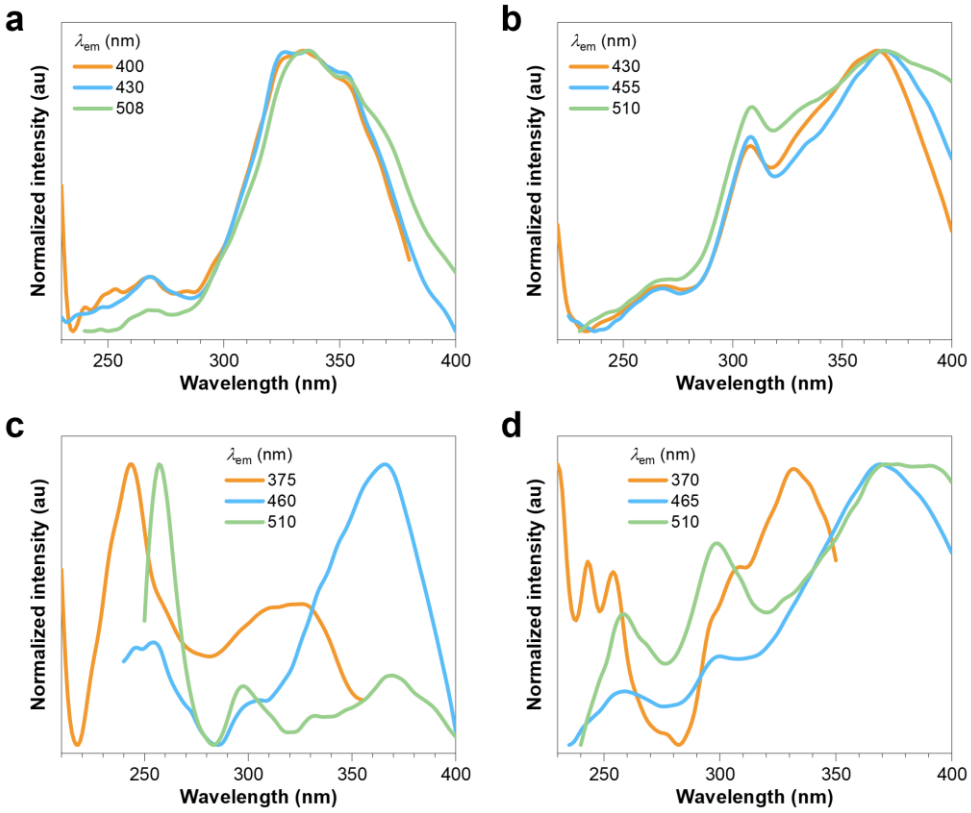

Fig. S41 Excitation spectra of (a,b)10-Br-a and (c,d) 10-Br-b polymorphic phase (a,c) II and (b,d) III measured at different λ_{em}s.

Table S4. Quantum yields of GAQASs polymorphs at 298 K.

Compound	λ_{ex} [nm]	Φ_f [%]	Φ_p [%]	Φ_c [%]
10-Br-a	254	2.0	1.1	3.1
	312	4.8	2.3	7.1
10-Br-a-phase II	254	1.6	0.7	2.3
	312	2.5	1.0	3.5
10-Br-a-phase III	254	0.5	0.6	1.1
	312	1.1	1.8	2.9
10-Br-b	254	2.7	8.8	11.5
	312	2.1	5.1	7.2
10-Br-b-phase II	254	2.0	4.3	6.3
	312	1.9	3.8	5.7
10-Br-b-phase III	254	0.6	1.8	2.4
	312	0.6	1.9	2.5
10-I-H_2O	254	0.01	0.79	0.8
	312	0.1	1.0	1.1
10-I-MeOH	254	0.3	1.4	1.7
	312	0.6	2.3	2.9
10-I-MeCN	254	1.2	3.0	4.2
	312	1.2	3.8	5.0
8-Br-a	254	5.4	2.9	8.3
	312	5.3	2.1	7.4
8-Br-b	254	11.2	11.2	22.4
	312	9.0	4.9	13.9

Table S5. Quantum yields of GAQASs polymorphs at 77 K.

Compound	$\Phi_{c,254}$ [%]	$\Phi_{c,312}$ [%]
10-Br-a	11.6	21.6
10-Br-b	21.1	17.1
10-I-H_2O	14.8	10.2
10-I-MeOH	20.7	12.1
10-I-MeCN	23.5	19.5

Table S6. Nanosecond scale lifetimes for GAQASs polymorphs at 298 K.

Compound	λ_{ex} [nm]	λ_{em} [nm]	τ_1 [ms]	A_1 [%]	τ_2 [ms]	A_2 [%]	τ_3 [ms]	A_3 [%]	τ [ns]
10-Br-a	254	395	5.7	100	/	/	/	/	5.7
	312	400	3.1	40.30	12.4	59.70	/	/	8.6
	365	430	2.6	37.13	10.0	62.87	/	/	7.3
10-Br-a-phase II	254	402	2.5	27.16	10.0	72.84	/	/	8.0
	312	403	3.4	36.98	13.0	63.02	/	/	9.4
	365	430	0.9	5.43	3.7	42.56	13.1	52.02	8.4
10-Br-a-phase III	254	430	4.5	100	/	/	/	/	4.5
	312	430	1.9	31.55	9.3	68.45	/	/	7.0
	365	445	1.7	26.60	5.8	73.40	/	/	4.7
10-Br-b	254	375	4.8	100	/	/	/	/	4.8
	312	378	2.0	33.09	7.4	66.91	/	/	5.6
	365	460	1.3	24.64	4.8	75.36	/	/	3.9
10-Br-b-phase II	254	370	4.9	100	/	/	/	/	4.9
	312	380	2.4	27.67	7.5	72.33	/	/	6.1
	365	465	0.8	12.21	3.7	87.79	/	/	3.4
10-Br-b-phase III	254	370	4.2	100	/	/	/	/	4.2
	312	390	2.4	42.68	6.8	57.32	/	/	4.9
	365	468	3.0	100	/	/	/	/	3.0
10-I-H_2O	254	355	0.3	25.57	3.4	74.43	/	/	2.6
	312	380	0.3	16.39	2.8	83.61	/	/	2.4
	365	470	1.6	100	/	/	/	/	1.6
10-I- MeOH	254	370	0.3	20.80	3.3	79.20	/	/	2.6
	312	380	1.7	34.78	5.4	65.22	/	/	4.2
	365	465	1.6	100	/	/	/	/	1.6
10-I-MeCN	254	365	0.3	21.61	3.3	78.39	/	/	2.7
	312	378	1.9	44.10	7.6	55.90	/	/	5.1
	365	468	2.1	100	/	/	/	/	2.1
8-Br-a	254	402	6.1	100	/	/	/	/	6.1
	312	405	2.9	34.00	12.2	66.00	/	/	9.0
	365	430	7.6	100	/	/	/	/	7.6
8-Br-b	254	430	2.3	21.24	9.2	78.76	/	/	7.8
	312	405	0.4	23.89	3.1	43.37	11.0	32.74	5.0
	365	440	0.3	10.93	2.4	36.23	10.7	52.84	6.6

Table S7. Millisecond scale lifetimes for GAQASs polymorphs at 298 K.

Compound	λ_{ex} [nm]	λ_{em} [nm]	τ_1 [ms]	A_1 [%]	τ_2 [ms]	A_2 [%]	τ_3 [ms]	A_3 [%]	τ_4 [ms]	A_4 [%]	τ [ms]
10-Br-a	254	515	14	5.76	99	29.98	409	65.26	/	/	297
	312	525	2	8.77	13	17.57	106	31.24	107	42.42	208
	365	550	2	9.48	8	24.41	42	28.59	205	37.51	91
10-Br-a-phase II	254	525	0.3	9.32	4	17.26	28	32.57	159	40.86	75
	312	535	1	9.58	9	26.78	46	38.27	186	25.36	67
	365	575	11	7.53	37	47.56	108	44.91	/	/	67
10-Br-a-phase III	254	520	1	13.71	14	31.79	140	54.50	/	/	81
	312	525	0.8	8.47	6	21.19	35	34.76	169	35.59	74
	365	540	0.7	13.86	4	27.67	18	31.26	90	27.20	31
10-Br-b	254	515	94	23.26	294	30.41	882	46.33	/	/	520
	312	530	7	0.50	55	15.50	170	34.87	510	49.13	318
	365	560	4	7.92	18	27.39	60	29.28	153	35.42	77
10-Br-b-phase II	254	515	2	2.78	22	9.36	144	29.17	639	59.69	424
	312	530	1	4.04	11	14.19	70	31.49	354	50.28	202
	365	570	0.5	4.77	3	15.4	15	32.75	76	47.08	41
10-Br-b-phase III	254	515	0.5	8.13	5	14.73	36	29.39	234	47.75	123
	312	520	0.6	8.61	4	23.56	27	37.07	136	30.76	53
	365	550	8	37.08	55	62.91	/	/	/	/	38
10-I-H_2O	254	535	5	14.16	20	44.84	60	41.00	/	/	34
	312	540	2	4.72	6	21.64	22	42.73	70	30.90	33
	365	575	0.6	1.49	3	21.03	9	41.24	29	36.23	15
10-I-MeOH	254	535	1	5.25	8	23.02	34	44.34	124	27.39	51
	312	540	1	6.77	9	26.59	41	44.74	153	21.9	55
	365	575	4	23.56	18	46.51	70	29.93	/	/	30
10-I-MeCN	254	530	1	4.60	11	21.51	52	43.98	216	29.92	90
	312	540	1	6.74	12	24.17	61	43.27	248	25.82	93
	365	580	5	19.12	21	44.56	91	36.32	/	/	44
8-Br-a	254	530	0.1	13.32	2	7.81	18	15.93	137	62.93	89
	312	545	0.4	6.51	4	11.95	30	24.56	161	56.98	100
	365	580	0.9	10.68	5	15.06	15	19.67	57	54.59	35
8-Br-b	254	515	27	10.24	92	44.63	292	45.13	/	/	176
	312	525	5	3.41	26	20.28	84	42.82	258	33.49	128
	365	545	1	3.55	9	11.72	44	38.51	168	46.22	96

Table S8. Millisecond scale lifetimes for two 10-Br polymorphs at 77 K.

Compound	λ_{ex} [nm]	λ_{em} [nm]	τ_1 [ms]	A_1 [%]	τ_2 [ms]	A_2 [%]	τ_3 [ms]	A_3 [%]	τ_4 [ms]	A_4 [%]	τ [ms]
10-Br-a	254	515	3	2.87	26	8.42	207	45.67	784	43.05	434
	312	530	3	4.41	26	10.14	216	48.77	757	36.68	386
	365	540	3	13.94	20	21.85	157	32.36	609	31.84	249
10-Br-b	254	505	4	6.55	36	16.95	224	33.50	1154	43.00	578
	312	525	4	8.75	26	20.93	138	36.27	650	34.05	277
	365	555	2	9.12	10	20.83	58	32.51	291	37.55	131

Table S9. Dynamic photophysical parameters of different polymorphic phases of 10-Br under 254 nm UV irradiation.

Compound	λ_f [nm]	λ_p [nm]	Φ_c [%]	Φ_f [%]	Φ_p [%]	τ_f [ns]	τ_p [ms]	k_{isc} [s^{-1}]	k_r^p [s^{-1}]	k_{nr}^p [s^{-1}]
10-Br-a-phase II	402	525	2.3	1.6	0.7	8.0	159	3.8×10^7	0.14	6.1
10-Br-a-phase III	430	525	1.1	0.5	0.6	4.5	140	1.2×10^8	0.08	7.1
10-Br-b-phase II	375	515	6.3	2.0	4.3	4.9	639	1.4×10^8	0.10	1.5
10-Br-b-phase III	375	515	2.4	0.6	1.8	4.2	234	1.8×10^8	0.10	4.2

$\Phi_c = \Phi_f + \Phi_p$; $\Phi_{isc} = \Phi_p/(\Phi_p + \Phi_f)$; $k_{isc} = \Phi_p/(\Phi_p + \Phi_f)\,\tau_f$; $k_r^p = (\Phi_p + \Phi_f)/\tau_p$; $k_{nr}^p = (1 - \Phi_p - \Phi_f)/\tau_p$. λ_f and λ_p are the PL maxima of fluorescence and phosphorescence of the polymorphs. Φ_c, Φ_f and Φ_p are the quantum efficiencies of total emission, fluorescence and phosphorescence of the polymorphs, respectively.

References

[1] M. D. Li, N. K. Wong, J. Xiao, R. Zhu, L. Wu, S. Y. Dai, F. Chen, G. Huang, L. Xu, X. Bai, M. R. Geraskina, A. H. Winter, X. Chen, Y. Liu, W. Fang, D. Yang and D. L. Phillips, *J. Am. Chem. Soc.*, 2018, **140**, 15957.

[2] T. Lu and F. Chen, *J. Comput. Chem.*, 2012, **33**, 580.

[3] T. Lu and Q. Chen, *J. Comput. Chem.*, 2022, **43**, 539.

[4] C. Lefebvre, G. Rubez, H. Khartabil, J. C. Boisson, J. Contreras-Garcia and E. Henon, *Phys. Chem. Chem. Phys.*, 2017, **19**, 17928.